Molecular Therapy
Nucleic Acids
Original Article

AhR/miR-23a-3p/PKCα axis contributes to memory deficits in ovariectomized and normal aging female mice

Shuai Zhang,[1,2] Xiaobin An,[1,2] Siyu Huang,[1] Lu Zeng,[1] Yi Xu,[1] Dan Su,[1] Yang Qu,[1] Xin Tang,[1] Jing Ma,[1] Junkai Yang,[1] and Jing Ai[1]

[1]Department of Pharmacology (The State-Province Key Laboratories of Biomedicine-Pharmaceutics of China), College of Pharmacy of Harbin Medical University, Harbin, Heilongjiang Province 150086, China

The mechanism of estrogen deficiency-induced cognitive impairment is still not fully elucidated. In this study, we assessed the effect of microRNA (miRNA) on the memory of long-term estrogen-deficient mice after ovariectomy (OVX) and normal aging. We observed that 5-month OVX and 22-month-old normal aging female mice showed significantly impaired spatial and object recognition memory, declined hippocampal long-term potentiation (LTP), and decreased hippocampal protein kinase C α (PKCα) protein. Quantitative real-time PCR analysis showed upregulated miRNA-23a-3p (miR-23a-3p) in the hippocampus of 5-month OVX and 22-month-old female mice. *In vitro*, overexpression of miR-23a-3p downregulated PKCα by binding the 3¿ UTRs of *Prkca* mRNAs, which was prevented by its antisense oligonucleotide AMO-23a. *In vivo*, adeno-associated virus-mediated overexpression of miR-23a-3p (AAV-pre-miR-23a-3p) suppressed hippocampal PKCα and impaired the memory of mice. Chromatin immunoprecipitation analysis showed that aryl hydrocarbon receptor (AhR) binds the promoter region of miR-23a-3p. The AhR-dependent downregulation of PKCα could be prevented by AMO-23a as well. Furthermore, knockdown of miR-23a-3p using AAV-AMO-23a rescued the cognitive and electrophysiological impairments of OVX and normal aging female mice. We conclude that long-term estrogen deficiency impairs cognition and hippocampal LTP by activating the AhR/miR-23a-3p/PKCα axis. The knockdown of miR-23a-3p may be a potentially valuable therapeutic strategy for estrogen deficiency-induced memory deficits.

INTRODUCTION

Estrogen (or 17β-estradiol), as a kind of crucial female hormone, plays essential roles in memory processing.[1,2] It has been found that estrogen deficiency impairs memory ability through enhancement of neuroinflammation, amyloidogenesis, and nuclear factor κB (NF-κB) activation.[3] In perimenopausal and postmenopausal females, hormone replacement therapy is also a popular way to delay estrogen deficiency-induced climacteric syndromes.[4] However, the internal molecular mechanisms of estrogen deficiency-induced cognitive impairment are still not fully understood. Further clarifying how estrogen depletion impairs cognition is necessary for precisely preventing the female cognitive decline following menopause or ovarian surgery.

Accumulating evidence indicates that protein kinase C (PKC) isozymes play essential roles in various phases or types of learning and memory.[5] PKC signaling deficit was even considered a mechanistic hypothesis for the origins of Alzheimer's disease (AD).[6] A recent study with fluorescence resonance energy transfer (FRET) indicated that PKCα, integrating spatiotemporally distinct Ca^{2+}, is activated robustly and rapidly in stimulated spines and is the only isozyme required for structural plasticity.[7] Selective blockade of PKCα inhibits the memory-specific increase of spine numbers.[8] PKCα mutation also promotes synaptic defects in AD.[9] But whether and how the estrogen deficiency dysregulates PKCα function is still not fully understood.

MicroRNAs (miRNAs) are involved in neuronal cell specification and patterning during development and also in higher cognitive processes, such as structural plasticity and memory formation in the adult brain.[10] Our previous studies have reported an overexpressed miRNA-23a-3p (miR-23a-3p) in the heart tissues of ovariectomy (OVX) models.[11,12] In addition, overexpression of miR-23a-3p is also involved in breast cancer, ovarian carcinoma, and leukemia.[13,14] Importantly, miR-23a-3p can regulate oligodendrocyte differentiation[15] and impair hippocampal neurons,[16] suggesting the potential effects of miR-23a-3p in the CNS. In the present study, by computational analysis of miRNAs, we found that miR-23a-3p carries a binding site in the 3¿ untranslated region (3¿ UTR) of PKCα and aryl hydrocarbon receptor (AhR), an estrogen depletion-sensitive protein,[17,18] is the upstream transcriptional factor of miR-23a-3p. Therefore, we hypothesized that long-term estrogen deficiency might

Received 28 October 2020; accepted 14 February 2021;
https://doi.org/10.1016/j.omtn.2021.02.015.

[2]These authors contributed equally

Correspondence: Jing Ai, Department of Pharmacology (The State-Province Key Laboratories of Biomedicine-Pharmaceutics of China), College of Pharmacy of Harbin Medical University, Harbin, Heilongjiang Province 150086, China.
E-mail: azhrbmu@126.com

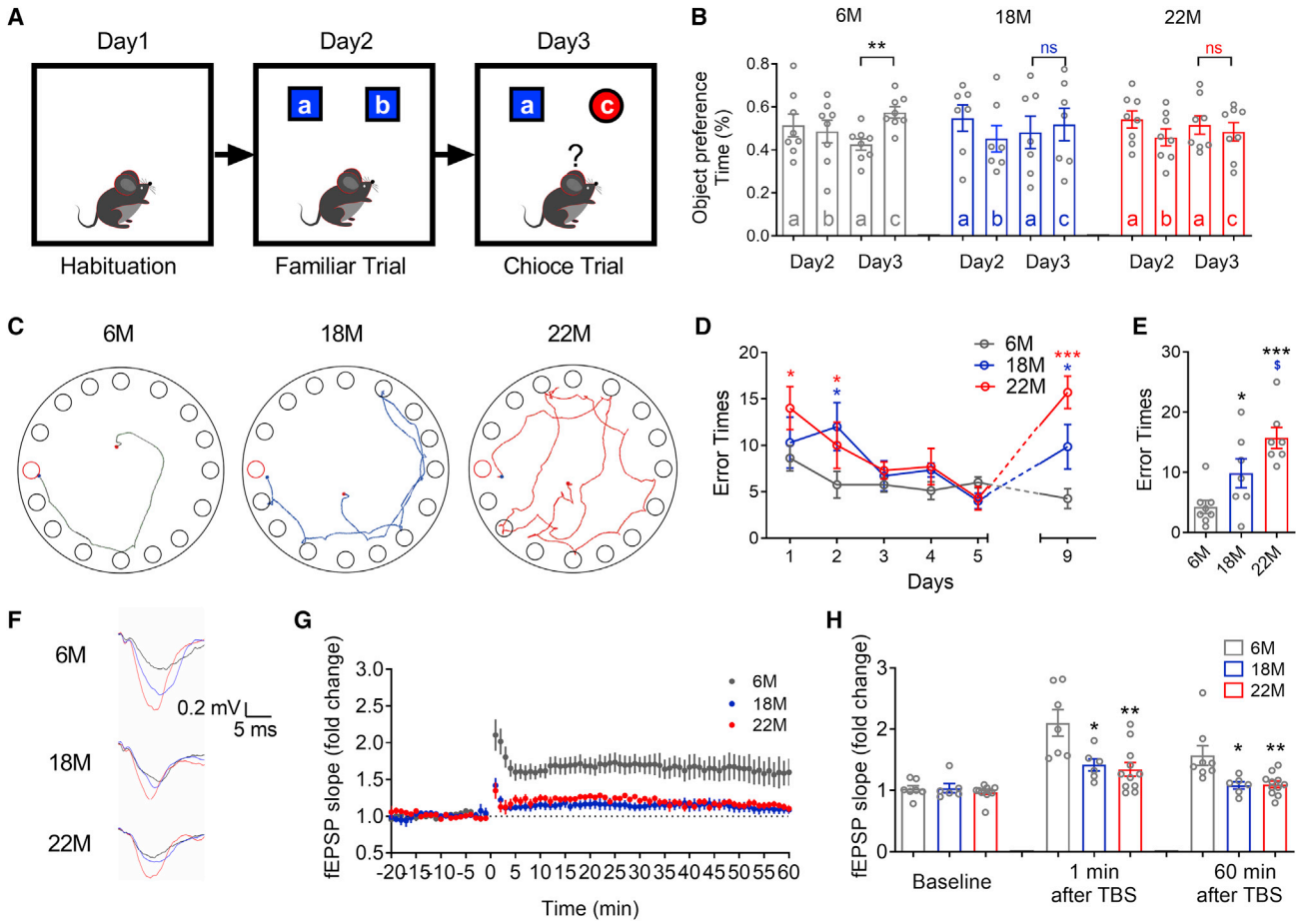

Figure 1. Age-dependent impairments of cognition and synaptic plasticity in female aging mice

(A) Diagram showing the procedure of the object recognition test. (B) Object preference calculated from exploring time for 6- (n = 8), 18- (n = 7), and 22- (n = 8) month-old mice. **p < 0.01 versus familiar object; ns, no statistical significance. (C) Representative path tracings of the probe test on day 9 in the Barnes maze test for each group. Typical exploring patterns indicated tending to the escape hole in 6-month-old mice, while random-type exploring paths were found in 18- and 22-month-old mice. (D) Comparison of average error times to find the escape hole for 6- (n = 8), 18- (n = 7), and 22- (n = 8) month-old mice on training days 1–6 and probe test day 9. (E) Bar graph showing comparison of average error times to find the escape hole for 6-, 18-, and 22-month-old mice on probe test day 9. (F) Sample hippocampal fEPSP traces of 6-, 18-, and 22-month-old mice during LTP. The black, red, and blue traces reflect the fEPSP at baseline, 1 min, and 60 min after TBS. (G) Time course graph showing recordings of C/A LTP. C/A fEPSPs exhibited a robust potentiation in the 6-month-old mice (n = 7) and mild potentiation in the 18- (n = 6) and 22- (n = 11) month-old mice. (H) Summary of the changes in C/A fEPSP slopes of 6-, 18-, and 22-month-old mice at baseline, 1 min, and 60 min after TBS. *p < 0.05 versus 6-month-old mice, **p < 0.01 versus 6-month-old mice, ***p < 0.001 versus 6-month-old mice, $p < 0.05 versus 18-month-old mice; ns, no statistical significance. Data in all graphs are presented as mean ± SEM.

impair the memory ability of female mice through activating the AhR/miR-23-3p/PKCα axis.

RESULTS

Age-dependent impairments of cognition and synaptic plasticity in female aging and OVX mice

The 18- and 22-month-old C57BL/6 mice are equivalent to 55 (average age of menopause)- and 70 (high incidence of AD)-year-old human beings, respectively.[19] Therefore, we first investigated the age-related changes of episodic and spatial memory of 6-, 18-, and 22-month-old female mice (Figure 1A). In contrast to the new object preference behavior of 6-month-old mice, 18- and 22-month-old mice displayed similar exploring time (Figure 1B) and frequency (Figure S1A) on familiar and novel objects during the object recognition task, which implied a quick episodic memory decline after the onset of menopause. Whereas the object recognition task cannot identify the severity of cognitive impairment, we thus next performed the Barnes maze test to assess the spatial memory of mice (Figure 1C). As predicted, 18- and 22-month-old mice displayed an age-dependent increase of error times (Figures 1D and 1E) and searching distance (Figures S1B and S1C) during the Barnes maze test. Consistent with the impaired new object recognition and spatial memory, we also discovered significant decreases of long-term potentiation (LTP) in the hippocampus of 18- and 22-month-old female mice after exposure to the LTP inducer theta burst

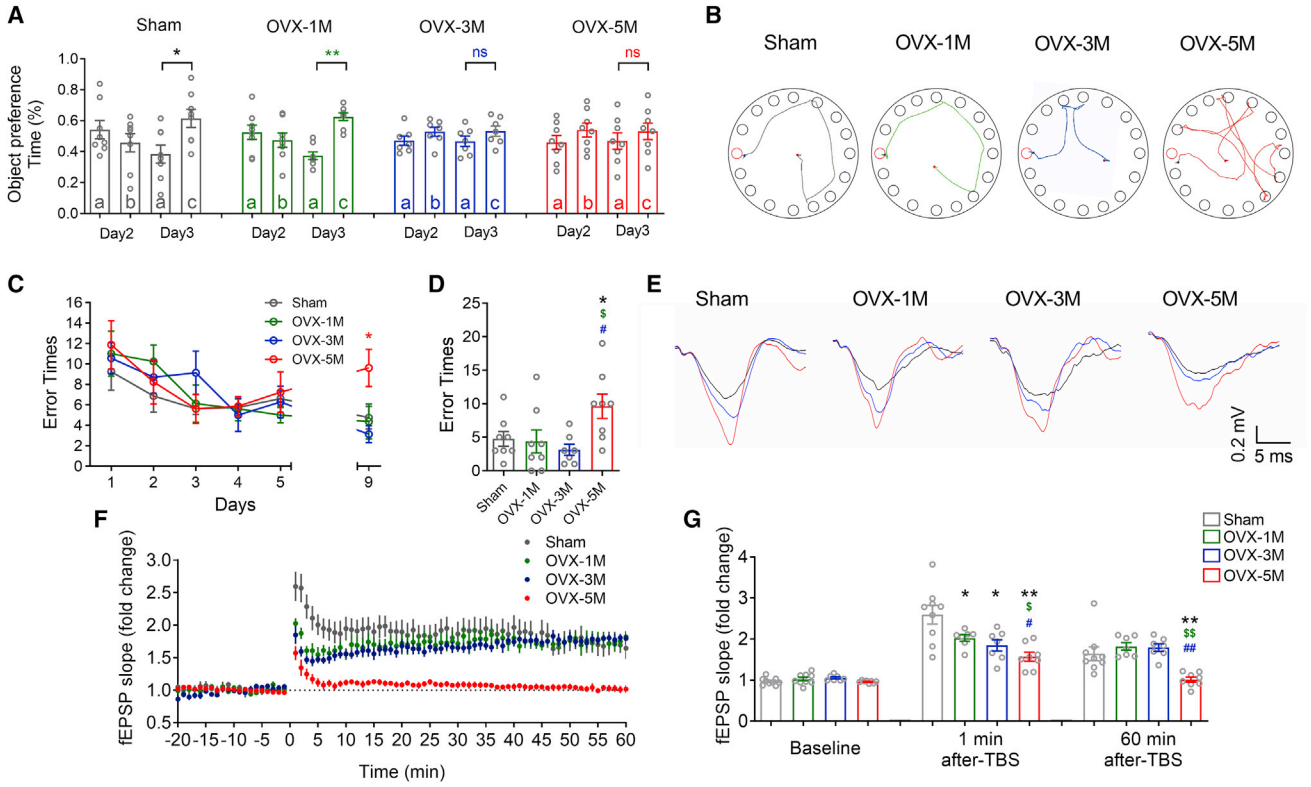

Figure 2. Long-term estrogen deficiency impairs the cognition of mice

(A) Object preference calculated from exploring time for Sham (n = 8), 1- (n = 8), 3- (n = 7), and 5- (n = 8) month OVX mice. *p < 0.05 versus familiar object, **p < 0.01 versus familiar object; ns, no statistical significance. (B) Representative path tracings of the probe test on day 9 in the Barnes maze test for each group. Typical exploring patterns indicated tending to the escape hole in Sham and 1 or 3 months after OVX surgery, while random-type exploring paths were found 5 months after OVX surgery. (C) Comparison of average error times to find the escape hole for Sham (n = 8), 1- (n = 8), 3- (n = 7), and 5- (n = 8) month OVX mice on training days 1–6 and probe test day 9. (D) Bar graph showing comparison of average error times to find the escape hole for Sham group and OVX group on probe test day 9. (E) Sample hippocampal fEPSP traces of Sham, 1- , 3- , and 5-month OVX mice during LTP. The black, red, and blue traces reflect the fEPSP at baseline, 1 min, and 60 min after TBS. (F) Time course graph showing recordings of C/A LTP. C/A fEPSPs exhibited a robust potentiation of Sham (n = 9) and 1- (n = 7), and 3- (n = 7) month OVX mice and mild potentiation in the 5-month (n = 8) OVX mice. (G) Summary of the changes in C/A fEPSP slopes of Sham and 1-, 3-, and 5-month OVX mice at baseline, 1 min of TBS, and 60 min after TBS. *p < 0.05 versus Sham mice, **p < 0.01 versus Sham mice, $p < 0.05 versus 1-month OVX mice, $$p < 0.01 versus 1-month OVX mice, #p < 0.05 versus 3-month OVX mice, ##p < 0.01 versus 3-month OVX mice; ns, no statistical significance. Data in all graphs are presented as mean ± SEM.

stimulation (TBS) (Figures 1F–1H). Given the previous reported preponderance of dementia among postmenopausal females compared with same-age males,[20] we considered that menopause is a risk factor for the cognitive impairment of aging mice.

To further clarify the role of estrogen in the cognitive decline of female mice, we established OVX mouse models with adult 2-month-old female mice and assessed their episodic and spatial memory after 1, 3, and 5 months of surgery. We found that 1-month OVX mice showed intact episodic and spatial memory (Figures 2A–2D; Figures S1D–S1F). Three months after OVX surgery, the mice displayed no preference (Figure 2A; Figure S1D) on the familiar and novel objects but did not show more errors (Figures 2B–2D) or longer total exploring distance (Figures S1E and S1F) in the probe trial of the Barnes maze test. However, when repeating the same behavioral tests in 5-month OVX mice, we observed that 5-month OVX mice show not only no preference for the new object in the object recognition task but also more error times and significantly longer exploring distance in the probe trials of the Barnes maze test (Figures 2B–2D; Figures S1D–S1F). These results demonstrated a time-dependent effect of estrogen deficiency on the impairment of episodic and spatial memory in female mice. Accordingly, we evaluated the hippocampal electrophysiological properties of OVX mice. The input-output curve showed intact CA1 responsiveness to Schaffer collateral (SC) stimulation following estrogen deficiency (Figures S2A–S2C). We then monitored the TBS-induced hippocampal LTP and observed a time-dependent decline of normalized field excitatory postsynaptic potential (fEPSP) slopes after 1–20 min of TBS in 1-, 3-, and 5-month OVX mice. However, only the declined normalized fEPSP slope in 5-month OVX mice continued to 60 min after TBS (Figures 2F and 2G). These results indicated that estrogen deficiency time-dependently impaired the cognition and synaptic plasticity of female mice.

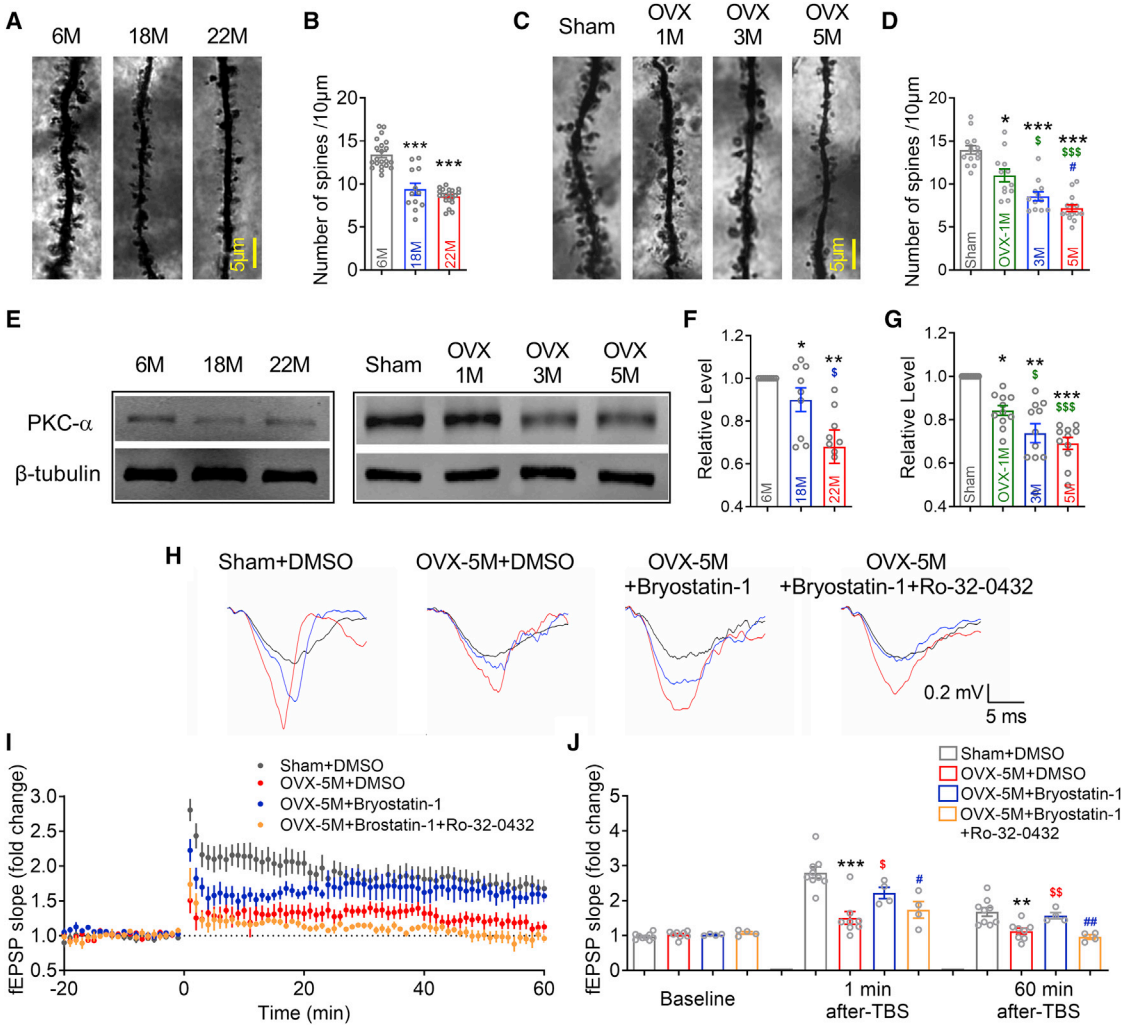

Figure 3. Long-term estrogen deficiency induces hippocampal PKCα loss of function

(A and B) Number of dendritic spines in CA1 region of 6- (n = 21), 18- (n = 12), and 22- (n = 22) month-old mice. ***p < 0.001 versus 6-month-old mice. (C and D) Number of dendritic spines in CA1 region of Sham and 1-, 3-, and 5-month OVX mice. *p < 0.05 versus Sham mice, ***p < 0.001 versus Sham mice, $p < 0.05 versus 1-month OVX mice, $$$p < 0.001 versus 1-month OVX mice, # p < 0.05 versus 3-month OVX mice. n = 12 neurons for each group. (E–G) western blot analysis with the hippocampus in 6- (n = 9), 18- (n = 9), and 22- (n = 9) month-old mice and Sham (n = 11), 1-month (n = 11), 3-month (n = 11), and 5-month (n = 11) OVX mice. *p < 0.05 versus 6M/Sham mice, *p < 0.01 versus 6-month-old/Sham mice, ***p < 0.001 versus 6-month-old/Sham mice, $p < 0.05 versus 18-month-old mice or 1-month OVX mice, $$$p < 0.001 versus 1-month OVX mice. (E) Representative immunoblotting images of PKCα and β-tubulin. (F and G) The digital data of the immunoblotting analysis. The optical density was evaluated for each band and normalized to 6-month-old/Sham mice after correction for protein loading with β-tubulin. (H) Sample fEPSP traces of Sham + DMSO, 5-month OVX + DMSO, 5-month OVX + bryostatin-1, and 5-month OVX + bryostatin-1 + Ro32-0432 hippocampal slices during LTP. The black, red, and blue traces reflect the fEPSP at baseline, 1 min, and 60 min after TBS. (I) Time course graph showing the C/A LTP of Sham + DMSO (n = 9), 5-month OVX + DMSO (n = 8), 5-month OVX + bryostatin-1 (n = 4), and 5-month OVX + bryostatin-1 + Ro32-0432 (n = 4) hippocampal slices. (J) Summary of the changes in C/A fEPSP slopes of Sham + DMSO, 5-month OVX + DMSO, 5-month OVX + bryostatin-1, and 5-month OVX + bryostatin-1 + Ro32-0432 hippocampal slices at baseline, 1 min of TBS, and 60 min after TBS. **p < 0.01 versus Sham + DMSO, ***p < 0.001 versus Sham + DMSO, $p < 0.05 versus 5-month OVX + DMSO, $$p < 0.01 versus 5-month OVX + DMSO, #p < 0.05 versus 5-month OVX + bryostatin-1, ##p < 0.01 versus 5-month OVX + bryostatin-1. Data in all graphs are presented as mean ± SEM.

Long-term estrogen deficiency downregulates PKCα expression in mice

The neural dendritic spine is the morphological basis of LTP and memory.[21] Therefore, we counted the hippocampal dendritic spines in aging female mice and OVX mice. We found a significantly decreased number of dendritic spines in the CA1 (Figures 3A and 3B) and dentate gyrus (DG) (Figures S3A and S3B) regions in both 18- and 22-month-old female mice. In addition, 1-, 3-, and 5-month OVX induced a time-dependent decrease of hippocampal dendritic spines in the CA1 (Figures 3C and 3D) and DG (Figures S3C and S3D) regions. The PKC isoenzymes have long been established as critical for synaptic plasticity.[22] It also has been found that PKC

activators reverse the neurological damage caused by ischemia and hypoxia.[23] Among PKC isozymes, PKCα concentrates in the hippocampus[24] and was recently reported as the only isozyme required for hippocampal structural plasticity.[7] We hence moved on to detect the hippocampal PKCα. As predicted, we observed decreased PKCα levels in the hippocampus of the aging female mice and OVX mice (Figures 3E–3G). However, in the other subtypes of the PKC family, except for a slight decrease of PKCβ, we did not observe changed PKCγ and PKCδ in the hippocampus of OVX mice (Figures S4A–S4C). To further confirm the crucial function of PKCα, we administrated 100 nmol of the PKCα activator bryostatin-1 to hippocampal slices from 5-month OVX mice. After 1 h of drug action, we found that the hippocampal LTP of 5-month OVX mice was rescued, and co-application of the selective PKCα inhibitor Ro-32-0432 offset the protective effect of bryostatin-1 (Figures 3H–3J). These results indicated that long-term estrogen deficiency downregulates hippocampal PKCα, which is essential for hippocampal synaptic plasticity.

Upregulated miR-23a-3p suppresses PKCα

We next explored the mechanism of PKCα downregulation following estrogen deficiency. Our previous study demonstrated that OVX-induced heart dysfunction of mice was controlled by upregulated heart miR-23a-3p expression.[11] miR-23a-3p is also the most obviously increased miRNA in the serum of postmenopausal women.[12] Here, we wanted to clarify whether miR-23a-3p participates in OVX-induced cognitive impairment in female mice. First, we conducted a computational analysis with the miRNA databases TargetScan and PicTar to identify the candidate miRNAs and surprisingly found that miR-23a-3p had a potential binding site in the 3¿ UTR of PKCα (739–745 bp) but not PKCβ, PKCγ, or PKCδ (Figure 4A). Thereafter, quantitative real-time PCR of the hippocampus showed a significant increase of miR-23a-3p in 3- and 5-month OVX mice (Figures 4B and 4C). Luciferase assay with the HEK293T cell line also verified that PKCα-encoding mRNA is a target of miR-23a-3p (Figures 4D–4F). Third, to observe whether changes of miR-23a-3p could affect PKCα expression *in vitro*, miR-23a-3p and AMO-23a were transfected by X-tremeGENE small interfering RNA (siRNA) transfection reagent into primary cultured neurons (Figure 4G). We observed that miR-23a-3p effectively inhibited the expression of PKCα, while AMO-23a rescued the downregulation of PKCα elicited by miR-23a-3p (Figure 4H). These data showed that miR-23a-3p could post-transcriptionally regulate PKCα expression via binding to the 3¿ UTR of PKCα mRNA at the site of 739–745 bp.

miR-23a-3p gain of function downregulates hippocampal PKCα and impairs mouse cognition *in vivo*

Since miR-23a-3p inhibited the expression of PKCα *in vitro*, we then sought to define whether overexpression of miR-23a-3p *in vivo* could inhibit PKCα and impair the cognition of mice. Therefore, we injected adeno-associated virus (AAV) with mis-pre-miR-23a-3p, pre-miR-23a-3p, or pre-miR-23a-3p + AMO-23a into the bilateral hippocampal CA1 of adult female mice, assessed their cognitive function 8 weeks later (Figure 5A), and confirmed the transduction efficiency with quantitative real-time PCR (Figure 5B). Western blot showed downregulated PKCα in miR-23a-3p overexpressed mice, which was reversed by the co-injection of AAV-AMO-23a (Figure 5C). Furthermore, we found that overexpression of miR-23a-3p significantly impaired spatial learning and memory, as indicated by increased error times (Figures 5D–5F) and longer exploring distance (Figures S5A and S5B) in the Barnes maze test. Overexpression of miR-23a-3p also impaired the object recognition memory of mice (Figure 5G; Figure S5C). By contrast, AMO-23a blocked the miR-23a-3p overexpression-induced cognitive impairment. After that, we detected the hippocampal LTP and found that miR-23a-3p overexpression significantly compromised hippocampal LTP, whereas AMO-23a reversed the impairment, which was similar to the action of PKCα activator bryostatin-1 (Figures 5H–5J).

AhR regulates miR-23a-3p transcription

To uncover the mechanisms underlying the miR-23a-3p upregulation, we analyzed the previous studies,[17,18] conducted computational analysis (Figure 6A), and finally considered that AhR might be a key regulator of miR-23a-3p transcription. We also employed chromatin immunoprecipitation (ChIP) analysis to test whether AhR could directly bind to the promoter region of miR-23a-3p. The results showed that AhR bound miR-23a-3p promoter at −1,963 to −995 bp upstream of the miR-23a-3p gene sequence (Figures 6B–6E). Previous studies reported that estrogen levels could affect the expression of AhR.[17,18] In the present immunoblot experiments, we found increased AhR in the hippocampus of both aged and OVX female mice (Figures 6F and 6G). Furthermore, we assessed the regulatory role of AhR on PKCα *in vitro* with primary cultured neurons. We used the classic AhR activator PCB-126 to activate AhR and found a decrease of PKCα (Figure 6H). To further verify that the AhR activation-induced downregulation of PKCα was dependent on the function of *miR-23a-3p*, we then applied AMO-23a to the primary cultured neurons with PCB-126, and we found that AMO-23a blocked the AhR activation-induced PKCα downregulation (Figure 6H). Combining the significant upregulated AhR in aging and OVX mice and the results of the ChIP assay, we collectively considered that long-term estrogen deficiency activated AhR, upregulated miR-23a-3p, and then downregulated PKCα.

MiR-23a-3p loss of function rescues hippocampal PKCα and memory of OVX and normal aging female mice

To further investigate the potential of AMO-23a as a future nucleic acid drug for estrogen deficiency-induced memory deficits, we injected AAV-AMO-23a into the bilateral hippocampus of 3-month OVX mice (Figure 7A). Eight weeks later, we found that AAV-AMO-23a injection reverted not only the increase of miR-23a-3p level (Figure 7B) but the reduction of hippocampal PKCα in OVX mice (Figure 7C). Importantly, knockdown of miR-23a-3p by injection of AAV-AMO-23a also rescued the spatial (Figures 7D–7F; Figures S6A and S6B) and new object recognition (Figure 7F; Figure S6C) memory and hippocampal LTP (Figures 7H–7J) in 5-month OVX mice. Moreover, we injected AAV-AMO-23a into the bilateral hippocampal CA1 of 18-month-old female mice.

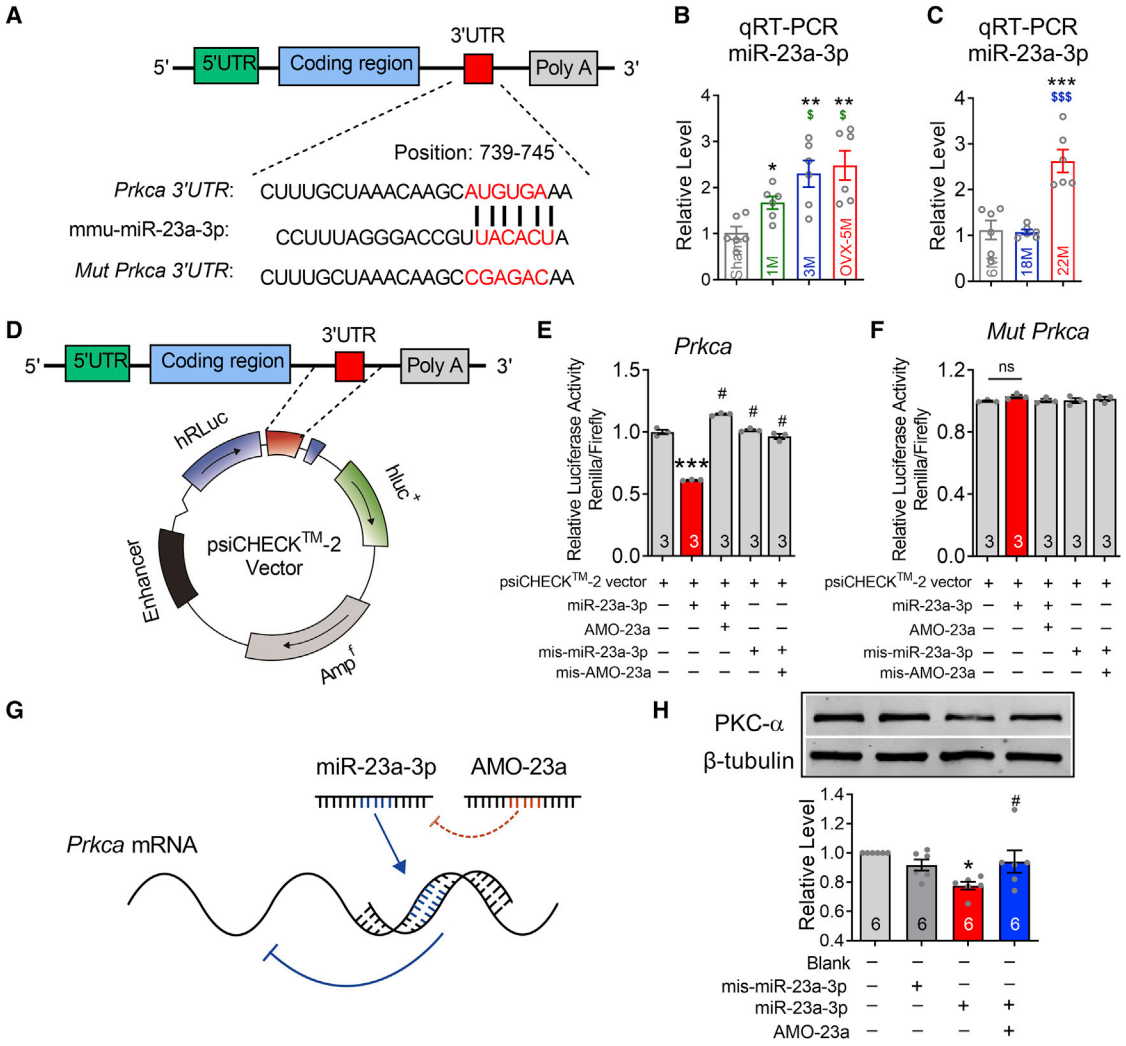

Figure 4. PKCα is a potential target of miR-23a-3p

(A) Complementarity between the miR-23a-3p seed sequence (5¿ end ~2–7 nucleotides) and the 3¿ UTR of mouse *Prkca* gene as predicted by a computational and bioinformatics-based approach using the TargetScan 5.1 algorithm. Watson-Crick complementarity is marked by a red color. (B) The levels of miR-23a-3p in the hippocampus of Sham and OVX mice as assessed by quantitative real-time PCR. *p < 0.05 versus Sham mice, **p < 0.01 versus Sham mice, $p < 0.05 versus 1-month OVX mice. n = 6 mice for each group. (C) The levels of miR-23a-3p in the hippocampus of 6-, 18-, and 22-month-old female mice as assessed by quantitative real-time PCR. ***p < 0.001 versus 6-month-old mice, $$$p < 0.001 versus 18-month-old mice. n = 6 mice for each group. (D) The mechanism of the luciferase assay. The full-length 3¿ UTR of *Prkca* was amplified by PCR and cloned into the psiCHECK-2-control vector. (E and F) Luciferase reporter gene assay for interactions between miR-23a-3p and its binding site (E) and the mutated binding site (F) in the 3¿ UTR of the *Prkca* gene in HEK293T cells. HEK293T cells were transfected with psiCHECK-2 vector, miR-23a-3p mimics, AMO-23a, or negative control siRNAs (mis-miR-23a-3p and mis-AMO-23a) using Lipofectamine 2000. ***p < 0.001 versus psiCHECK-2-control vector; #p < 0.05 versus miR-23a-3p; ns, no statistical significance. n = 3 batches of cells for each group. (G) Schematic diagram of miR-23a-3p silencing using antisense antagonist. miR-23a-3p binds to complementary target sites in the 3¿ UTRs of *Prkca* gene, which could be blocked by its antisense antagonist AMO-23a. (H) Expression of PKCα protein in primary cultured neurons was downregulated by miR-23a-3p determined by western blot analysis. *p < 0.05 versus mis-miR-23a-3p, #p < 0.05 versus miR-23a-3p. n = 3 batches of cells for each group. Data in all graphs are presented as mean ± SEM.

Four months later, the increased miR-23a-3p in the hippocampus of aged mice was prevented by injection of AAV-AMO-23a (Figure 8A). Accordingly, we found that miR-23a-3p knockdown rescued the hippocampal PKCα expression (Figure 8B) and spatial learning ability (Figures 8C–8E; Figures S6D and S6E) but not the new object recognition memory (Figures S6F and S6G) of 22-month-old female mice. Field recording of hippocampal slices revealed that the impaired hippocampal LTP in aged female mice was also reverted by AAV-AMO-23a (Figures 8F–8H). Collectively, these results suggested that knockdown of miR-23a-3p rescued the hippocampal PKCα and cognitive function of OVX and normal aging female mice.

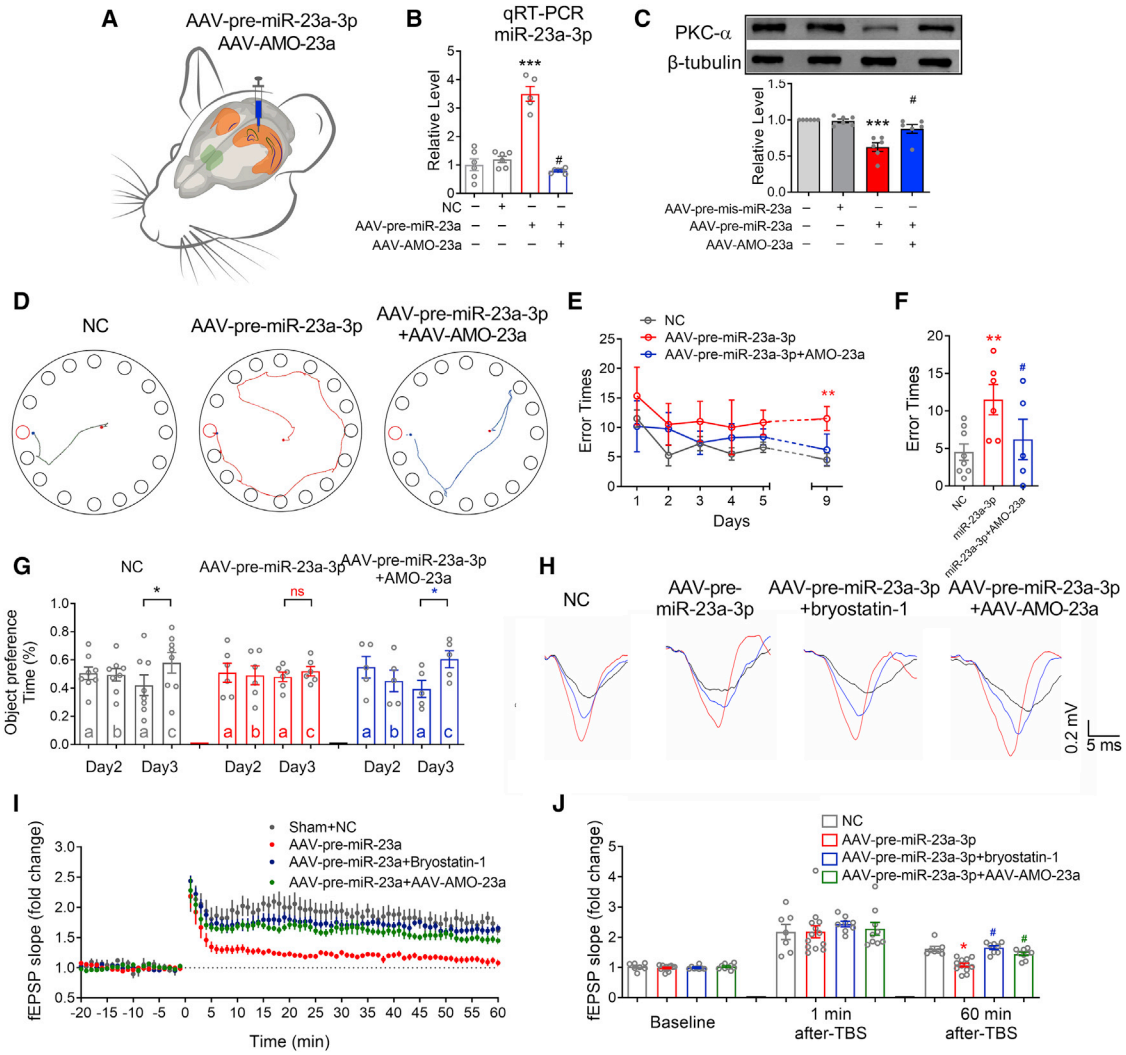

Figure 5. MiR-23a-3p gain of function impairs cognition and hippocampal synaptic plasticity of mice

(A) Schematic diagram of stereotactic adeno-associated virus injection into CA1 region of hippocampus. (B) The levels of miR-23a-3p in the hippocampus of AAV-NC-, AAV-pre-miR-23a-3p-, and AAV-pre-miR-23a-3p + AAV-AMO-23a-injected mice as assessed by quantitative real-time PCR. n = 6 mice for each group. (C) miR-23a-3p gain of function by injection of AAV-pre-miR-23a-3p represses the protein level of PKCα in hippocampi, which was prevented by AAV-AMO-23a. n = 6 mice for each group. (D) Representative path tracings of the probe test on day 9 in the Barnes maze test for each group. (E) Comparison of average error times to find the escape hole for AAV-NC (n = 8)-, AAV-pre-miR-23a-3p (n = 6)-, and AAV-pre-miR-23a-3p + AAV-AMO-23a (n = 5)-injected mice on training days 1–6 and probe test day 9. (F) Bar graph showing comparison of average error times to find the escape hole for AAV-NC-, AAV-pre-miR-23a-3p-, and AAV-pre-miR-23a-3p + AAV-AMO-23a-injected mice on probe test day 9. (G) Object preference calculated from exploring time for AAV-NC (n = 8)-, AAV-pre-miR-23a-3p (n = 6)-, and AAV-pre-miR-23a-3p + AAV-AMO-23a (n = 5)-injected mice. *$p < 0.05$ versus familiar object; ns, no statistical significance. (H) Sample hippocampal fEPSP traces of AAV-NC-, AAV-pre-miR-23a-3p-, AAV-pre-miR-23a-3p + bryostatin-1-, and AAV-pre-miR-23a-3p + AAV-AMO-23a-injected mice during LTP. The black, red, and blue traces reflect the fEPSP at baseline, 1 min, and 60 min after TBS. (I) Time course graph showing the C/A LTP of AAV-NC (n = 7)-, AAV-pre-miR-23a-3p (n = 12)-, AAV-pre-miR-23a-3p + bryostatin-1 (n = 8)-, and AAV-pre-miR-23a-3p + AAV-AMO-23a (n = 9)-injected mice. (J) Summary of the changes in C/A fEPSP slopes of AAV-NC-, AAV-pre-miR-23a-3p-, AAV-pre-miR-23a-3p + bryostatin-1-, and AAV-pre-miR-23a-3p + AAV-AMO-23a-injected mice at baseline, 1 min after TBS, and 60 min after TBS. *$p < 0.05$ versus AAV-NC mice, **$p < 0.01$ versus AAV-NC mice, ***$p < 0.001$ versus AAV-NC mice, $^{\#}p < 0.05$ versus AAV-pre-miR-23a-3p mice; ns, no statistical significance. Data in all graphs are presented as mean ± SEM.

DISCUSSION

The results of this study highlight how long-term estrogen deficiency induces cognitive impairment in OVX and normal aging female mice. We observed downregulated hippocampal PKCα in OVX and normal aging female mice, which raised the question of the mechanistic reason for PKCα loss of function. We were intrigued to find that miR-23a-3p has a binding site with the 3¿ UTR of PKCα, and AhR is the upstream transcriptional factor of miR-23a-3p. We were interested in determining whether the AhR/miR-23a-3p/PKCα axis contributes to memory deficits in OVX and normal aging female mice.

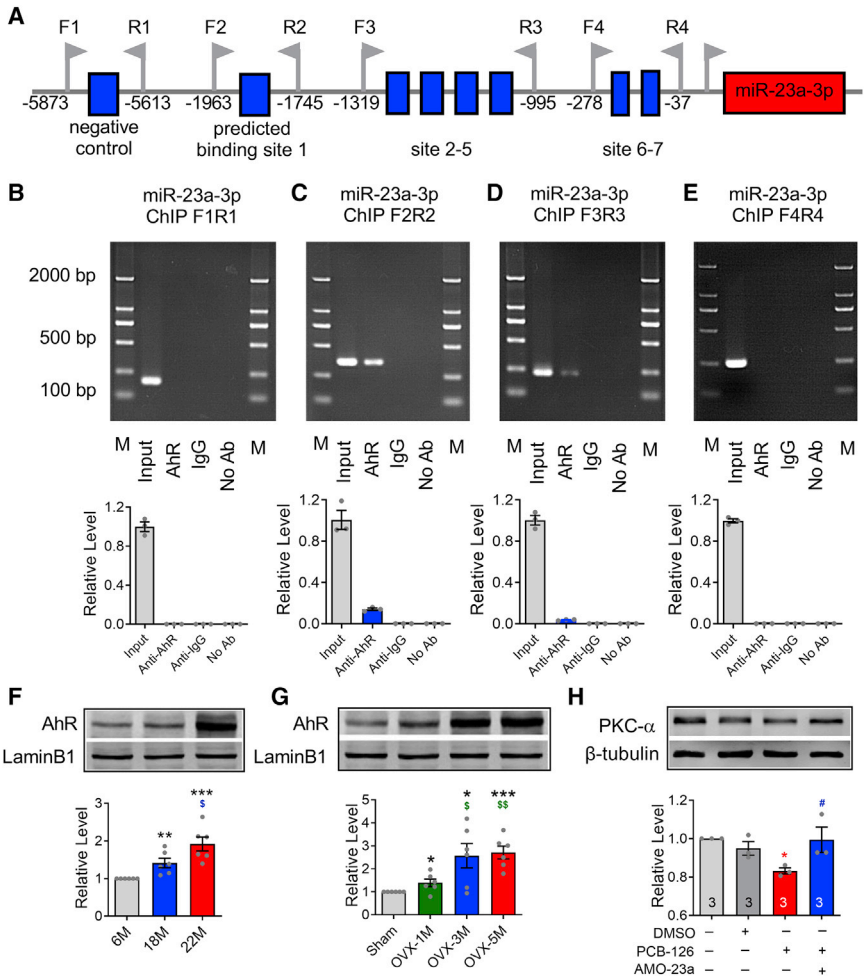

Figure 6. AhR regulates miR-23a-3p transcription

(A) Schematic representation of the upstream region of the mouse miR-23a-3p. The conservative AhR targeting sites are marked by a box. The primers for ChIP assay are underlined. (B–E) ChIP analysis of AhR binding to the promoter between −5,873 and −37 bp. ChIP assay was performed with hippocampal neuron. The anti-IgG antibody and no antibody treatments were used as negative control. The anti-AhR antibody was used to target specific immunoprecipitation. AhR binding to these target sites activates miR-23a-3p promoter activity. Bottom panels: qPCR analysis of AhR binding sequences (n = 3). (F and G) Top panels: Representative immunoblotting images of nuclear AhR and laminB1. Bottom panels: The digital data of the immunoblotting analysis. The optical density was evaluated for each band and normalized to 6M/Sham mice after correction for protein loading with laminB1. *$p < 0.05$ versus 6-month-old/Sham mice, **$p < 0.01$ versus 6-month-old/Sham mice, ***$p < 0.001$ versus 6-month-old/Sham mice, $^{\$}p < 0.05$ versus 18-month-old/OVX-1-month-old mice, $^{\$\$}p < 0.01$ versus 18-month-old/OVX-1 month mice. n = 6 mice for each group. (H) Downregulation of PKCα protein expression induced by PCB-126, which was reversed by AMO-23a transfection. *$p < 0.05$ versus DMSO-treated neuron, $^{\#}p < 0.05$ versus PCB-126-treated neuron. n = 3 batches of cells for each group. Data in all graphs are presented as mean ± SEM.

In the current study, we observed that estrogen deficiency time-dependently impaired the new object recognition and spatial memory of mice. The sequential impairment of object recognition memory and spatial memory of OVX and aging mice were similar to that of the AD mouse model.[25] Estrogen has previously been reported to modulate the activity of PKC in rat pituitary and preoptic area.[26,27] However, which PKC isoform and whether or how PKC participates in estrogen deficiency-induced neurodegenerative changes are still poorly understood. Here, consistent with the results of behavioral tests, we found downregulated hippocampal PKCα in normal aging and 5-month OVX female mice.

Our previous studies have shown that miR-23a-3p upregulation participates in estrogen deficiency-induced cardiac dysfunction.[11,12] Also, miR-23a-3p has been reported to induce telomere shortening and cellular senescence.[28,29] In the present study, we found a robustly increased hippocampal miR-23a-3p following long-term estrogen deficiency. The following *in vitro* and *in vivo* results also support the role for miR-23a-3p as an endogenous risk factor of memory deficits. By contrast, the knockdown of hippocampal miR-23a-3p with AAV-AMO-23a rescued the cognitive and electrophysiological impairments of 5-month OVX as well as aging female mice, whereas miR-23-3p knockdown from 18-month-old mice cannot attenuate the impairment of object recognition memory of 22-month-old mice. We considered that this might be due to the severe impairment of object recognition memory. In the present work, we knocked down the expression of miR-23a-3p of 3-month OVX mice and 18-month-old female mice. Three months after OVX surgery is the first time to see the impairment of object recognition memory in OVX mice. However, according to a previous publication, the impairment of object recognition memory could be observed in 15-month-old wild-type mice.[30] That is to say, the 18-month-old mice have already suffered the impairment of object recognition memory for at least 3 months, which is considered the main reason for the failed reversion of object recognition memory of 22-month-old mice. And this phenomenon also suggests that the miR-23a-3p/PKCα axis is just part of the mechanism of female aging-related cognitive impairment. The time window of AMO-23a therapy still needs discussion. Previous studies have demonstrated that uterine AhR mRNA increases after 2-week OVX, whereas the protein level of AhR might be decreased.[17,18] However, whether the hippocampal AhR protein level is changed after long-term OVX is still unknown. Here, we are the first to report that the hippocampal AhR was increased in estrogen deficiency mice. And the AhR activation-dependent downregulation of PKCα also relies on the function of miR-23a-3p. Collectively, we

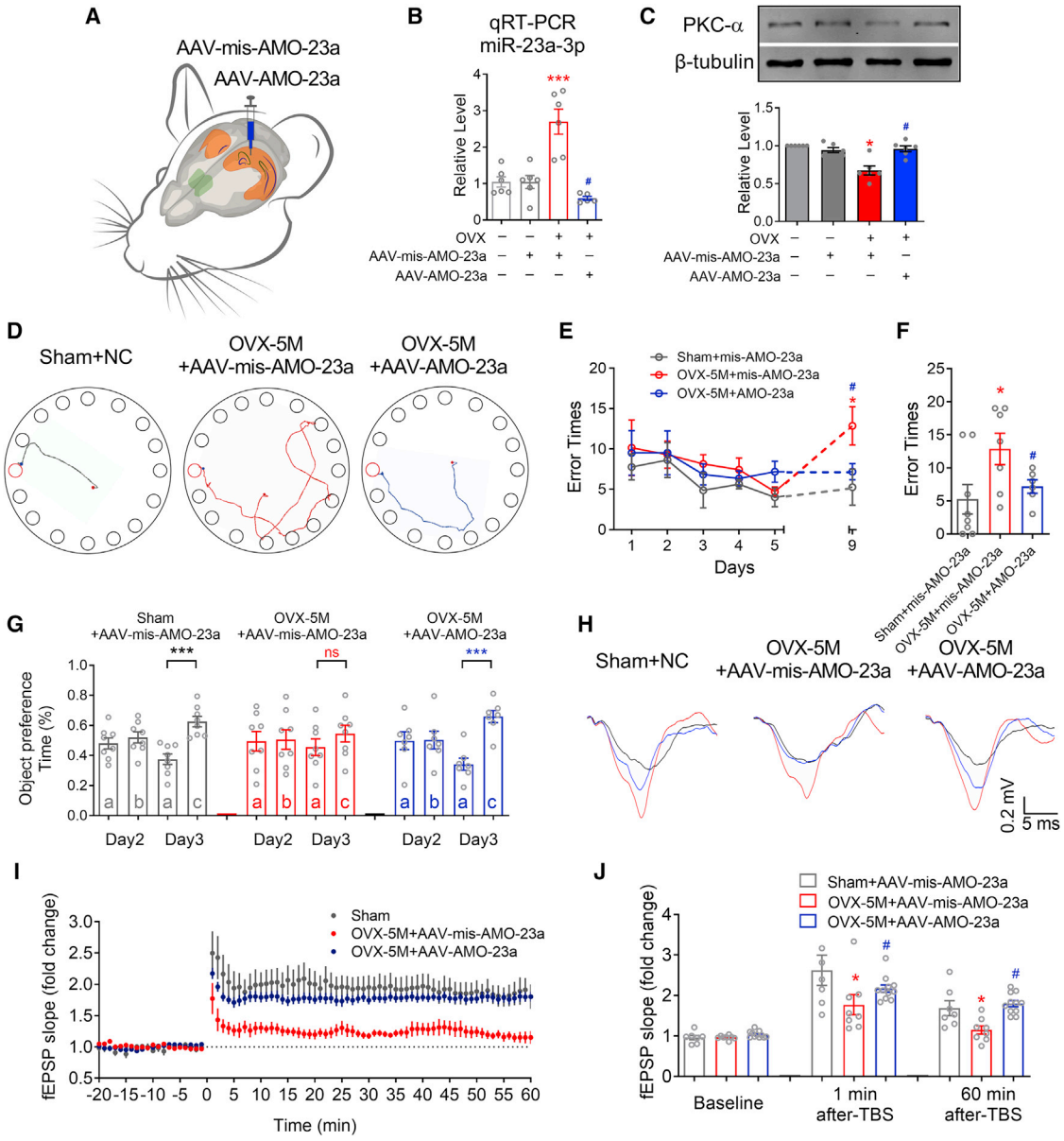

Figure 7. Knockdown of miR-23a-3p rescues cognition and hippocampal synaptic plasticity of 5-month OVX mice

(A) Schematic diagram of stereotactic adeno-associated virus injection into CA1 region of hippocampus. (B) The levels of miR-23a-3p in the hippocampus of Sham (n = 6), Sham + AAV-mis-AMO-23a (n = 6), OVX-5M + AAV-mis-AMO-23a (n = 6), and OVX-5M + AAV-AMO-23a (n = 5) mice as assessed by quantitative real-time PCR. (C) Knockdown of miR-23a-3p by injection of AAV-AMO-23a rescues the protein level of hippocampal PKCα in 5-month OVX mice. n = 6 mice for each group. (D) Representative path tracings of the probe test on day 9 in the Barnes maze test for each group. (E) Comparison of average error times to find the escape hole for Sham + AAV-mis-AMO-23a mice (n = 8), OVX + AAV-mis-AMO-23a mice (n = 8), and OVX + AAV-AMO-23a mice (n = 7) on training days 1–6 and probe test day 9. (F) Bar graph showing comparison of average error times to find the escape hole for Sham + AAV-mis-AMO-23a mice, OVX + AAV-mis-AMO-23a mice, and OVX + AAV-AMO-23a mice on probe test day 9. (G) Object preference calculated from exploring time for Sham+AAV-mis-AMO-23a mice (n = 8), OVX + AAV-mis-AMO-23a mice (n = 8), and OVX + AAV-AMO-23a (n = 7) mice. ***p < 0.001 versus familiar object; ns, no statistical significance. (H) Sample hippocampal fEPSP traces of Sham + AAV-mis-AMO-23a, OVX + AAV-mis-AMO-23a, and OVX + AAV-AMO-23a mice during LTP. The black, red, and blue traces reflect the fEPSP at baseline, 1 min, and 60 min after TBS. (I) Time course graph showing the C/A LTP of Sham + AAV-mis-AMO-23a mice (n = 8), OVX + AAV-mis-AMO-23a mice (n = 7), and OVX + AAV-AMO-23a mice (n = 11). (J) Summary of the changes in C/A fEPSP slopes of Sham + AAV-mis-AMO-23a mice, OVX + AAV-mis-AMO-23a mice, and OVX + AAV-AMO-23a mice at baseline, 1 min after TBS, and 60 min after TBS. *p < 0.05 versus Sham + AAV-mis-AMO-23a mice, ***p < 0.001 versus Sham + AAV-mis-AMO-23a mice, #p < 0.05 versus OVX-5M + AAV-mis-AMO-23a mice; ns:, no statistical significance. Data in all graphs are presented as mean ± SEM.

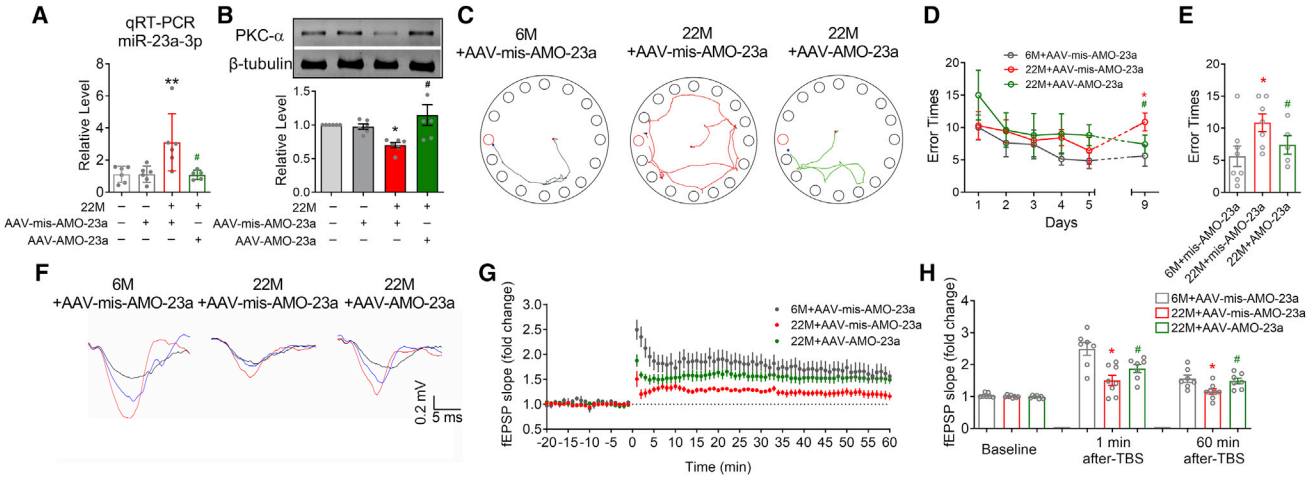

Figure 8. Knockdown of miR-23a-3p rescues cognition and hippocampal synaptic plasticity of aging female mice

(A) The levels of miR-23a-3p in the hippocampus of 6M (n = 6), 6M + AAV-mis-AMO-23a (n = 6), 22-month-old + AAV-mis-AMO-23a (n = 6), and 22-month-old + AAV-AMO-23a (n = 5) mice were assessed by quantitative real-time PCR. (B) Knockdown of miR-23a-3p by injection of AAV-AMO-23a rescues the protein level of hippocampal PKCα in 22-month-old female mice. n = 6 mice for each group. (C) Representative path tracings of the probe test on day 9 in the Barnes maze test for each group. (D) Comparison of average error times to find the escape hole for 6-month-old + AAV-mis-AMO-23a, 22-month-old + AAV-mis-AMO-23a, and 22-month-old + AAV-AMO-23a mice on training days 1–6 and probe test day 9. (E) Bar graph showing comparison of average error times to find the escape hole for 6-month-old + AAV-mis-AMO-23a (n = 8), 22-month-old + AAV-mis-AMO-23a (n = 7), and 22-month-old + AAV-AMO-23a (n = 5) mice on training days 1–6 and probe test day 9. (F) Sample hippocampal fEPSP traces of 6-month-old + AAV-mis-AMO-23a, 22-month-old + AAV-mis-AMO-23a, and 22-month-old + AAV-AMO-23a mice during LTP. The black, red, and blue traces reflect the fEPSP at baseline, 1 min, and 60 min after TBS. (G) Time course graph showing the C/A LTP of 6-month-old + AAV-mis-AMO-23a (n = 7), 22-month-old + AAV-mis-AMO-23a (n = 8), and 22-month-old + AAV-AMO-23a (n = 7) mice. (I) Summary of the changes in C/A fEPSP slopes of 6-month-old + AAV-mis-AMO-23a, 22-month-old + AAV-mis-AMO-23a, and 22-month-old + AAV-AMO-23a mice at baseline, 1 min after TBS, and 60 min after TBS. *$p < 0.05$ versus 6-month-old + AAV-mis-AMO-23a mice, **$p < 0.01$ versus 6-month-old + AAV-mis-AMO-23a mice, #$p < 0.05$ versus 22-month-old + AAV-mis-AMO-23a mice; ns, no statistical significance. Data in all graphs are presented as mean ± SEM.

propose an estrogen-AhR-miR-23a-3p-PKCα pathway, which plays a key role in the estrogen deficiency-induced cognitive impairments.

Circulating miRNAs have been reported to be associated with pathophysiological states, such as different types of cancer, heart diseases, oxidative liver injury, sepsis, pregnancy, and so on.[31–35] Some studies have reported correlations between peripheral miRNA expression levels and human cognitive impairment.[36,37] In our previous study, increased miR-23a-3p in the blood of postmenopausal women compared with matched control subjects was determined.[12] These findings are in line with our data from OVX mouse models indicating miR-23a-3p to be an endogenous risk factor of cognitive impairment and suggest miR-23a-3p as a possible biomarker for cognitive impairment of postmenopausal women and possibly for the response to treatment.

The pathogenesis of estrogen deficiency-induced cognitive impairment is very complex, and the detailed mechanisms of this process remain to be investigated. We have, for the first time, performed detailed experimental characterization to uncover the role of AhR/miR-23a-3p/PKCα in estrogen deficiency-induced cognitive impairment. However, it cannot rule out that other targets of miR-23a-3p might contribute to the estrogen deficiency-induced cognitive impairment. Actually, one miRNA usually has multiple target mRNAs, and PKC is only one of the targets of miR-23a-3p. Combining the computational prediction from TargetScan and the previously published memory-related protein, we considered that serotonin receptor 2A/2C,[38] CREB binding protein,[39] eukaryotic translation initiation factor 1/3/4,[40] metabotropic glutamate receptor 5,[41] and neurexin1/3[42] might have the potential to participate in the memory deficits of OVX and normal aging female mice. Thus, we need to identify the targetome of miR-23a-3p in the CNS of both OVX and female aging mice in future studies, which will provide a more comprehensive and accurate understanding of the role of miR-23a-3p in female aging. In addition to PKCα, we also observed decreased PKCβ, which is also a memory-related protein[5] but not the target of miR-23a-3p, in the hippocampus of OVX mice. The internal mechanism of PKCβ downregulation following estrogen deficiency deserves future discussion.

To conclude, we propose that the AhR/miR-23a-3p/PKCα axis participates in estrogen deficiency-induced memory deficits in OVX and aging female mice. The knockdown of miR-23a-3p rescues the learning and memory ability of estrogen deficiency mice. These findings may pave the way for a better understanding of the mechanism of estrogen deficiency-induced cognitive impairment and lead to the development of more effective treatments and biomarkers.

MATERIALS AND METHODS

Animals and treatment

Adult female C57BL/6 mice (age as described in Results) were housed under standard conditions (temperature 23 ± 1°C; humidity

55%–60%). Animals were maintained on a 12-h dark-light artificial cycle, with food and water *ad libitum*. OVX surgery was performed as previously described.[11,43] Samples for western blot and quantitative PCR (qPCR) were obtained after the experimental mice had been anesthetized with sodium pentobarbital (100 mg/kg, intraperitoneally [i.p.]). All animal procedures were approved by the Institutional Animal Care and Use Committee at Harbin Medical University (no. HMUIRB-2008-06) and the Institute of Laboratory Animal Science of China (A5655-01). All procedures conformed to Directive 2010/63/EU of the European Parliament.

Behavioral test

Novel object recognition[44,45] and Barnes maze[46] tests were performed as previously described. Detailed information can be found in the Supplemental materials and methods.

Western blotting

Western blotting was performed as previously described.[47] Detailed information can be found in the Supplemental materials and methods.

Quantitative real-time PCR

Quantitative real-time PCR was performed as previously described.[48] Detailed information can be found in the Supplemental materials and methods.

Golgi staining

Golgi staining was performed as previously described.[48] Detailed information can be found in the Supplemental materials and methods.

Electrophysiology

Acute hippocampal slice preparation

Hippocampal slices were prepared as previously described.[49] Detailed information can be found in the Supplemental materials and methods.

Extracellular recordings

A concentric bipolar microelectrode (CBARC75, FHC, Bowdoin, ME, USA) was placed in the SC domain at a 300 μm distance away from recording pipettes. Extracellular recordings were made in the stratum radiatum of CA1 area with recording pipettes that were pulled from borosilicate glass (BF100-58-10, Sutter Instrument, Novato, CA, USA) with resistances of 2–3 macrophages when filled with a NaCl (3 mol/L) solution. fEPSPs of SC-CA1 were evoked by current stimuli with stimulatory isolator ISO-Flex (AMPI, Jerusalem, Israel) controlled by Master-8 pulse generator (AMPI, Jerusalem, Israel). Analog signals were bypass filtered and digitized at 6 kHz with a Digidata 1550A and pCLAMP 10 software (Molecular Devices, San Jose, CA, USA). A stimulus intensity that evoked ~30% of the maximal fEPSP was used for LTP induction. Baseline stimulation was delivered every 30 s for at least 20 min before LTP induction to ensure stability of the response. LTP was induced by TBS (4 pulses at 100 Hz, with the bursts repeated at 5 Hz and each tetanus including three 10-burst trains separated by 15 s). Responses were recorded for 1 h after induction of LTP.[50] All electrophysiological data were collected with pCLAMP software (Molecular Devices, San Jose, CA, USA) and analyzed blindly.

Synthesis of miR-23a-3p, AMO-23a, and other oligonucleotides

MiR-23a-3p mimics (5¿-AUCACAUUGCCAGGGAUUUCC-3¿) and AMO-23a (5¿-GGAAAUCCCUGGCAAUGUGAU-3¿) were synthesized by GenePharma (Shanghai, China). AMO-23a contains 2-O-methyl modifications. In addition, a scrambled RNA was used as a negative control (NC) (5¿-UUCUCCGAACGUGUCACGUAA-3¿). All the synthesized oligonucleotides at both ends of the antisense molecules were locked by a methylene bridge connecting between the 2-O and the 4-C atoms.

Cell culture and treatment

Primary hippocampal and cortical neurons were cultured as previously reported.[51] Detailed information can be found in the Supplemental materials and methods.

Dual luciferase reporter assay

The dual luciferase reporter assay was performed as previously reported.[51] Detailed information can be found in the Supplemental materials and methods.

Chromatin immunoprecipitation assay

Before ChIP assay, the promotor sequence of miR-23a-3p was extracted from UCSC Genome Browser, and the promotor sequence of miR-23a-3p was then input into the JASPAR database for the prediction of transcriptional factors. Thirty-two putative binding sites were predicted between AhR and the promotor sequence of miR-23a-3p. Subsequently, ChIP assay was performed with primary cultured neurons using the Imprint ChIP assay kit (catalog no. 26156; Pierce Thermo Fisher Scientific) according to the manufacturer's instructions. The PCR primers (miR-23a-3p ChIP forward [F] primer 1: 5′-CCAGAAGAGGGAGTCAGATC-3′; miR-23a-3p ChIP reverse [R] primer 1: 5′-TGTCATGCACAAAGACCAGAC-3′; miR-23a-3p ChIP F2: 5′-GATAGCTGTGCTTGTCATGTAG-3′; miR-23a-3p ChIP R2: 5′-GAGAAGGTATTTAGCACCCAG-3′; miR-23a-3p ChIP F3: 5′-TGGAAGTAGAGGAGGGCTAG-3′; miR-23a-3p ChIP R3: 5′- TAGCACCTAAAGAGAGAAAG-3′) were designed to amplify 218, 324, and 241 bp fragments, respectively, from selected genomic regions. RT-PCR of genomic regions containing the putative AhR-binding sites was performed in triplicate. Cycling parameters were 98°C for 5 min, followed by 35 cycles of 98°C for 30 s, 55°C for 20 s, 68°C for 20 s, and 72°C for 5 min. Amplification of the negative control construct, a 260 bp fragment spanning selected genomic regions, was performed with oligos 5¿-GGAAGGACAGC ATCATGCCG-3¿ and 5¿-ATTATTCCCAGGCCCAAAGC-3¿. The relative occupancy of the immunoprecipitated factor at a locus was estimated by using the comparative threshold method.

Viral vector construction and injection

The synthesis and AAV packaging of single-stranded DNA oligonucleotides including NC, pre-miR-23a-3p, AMO-23a, and

mis-AMO-23a sponge were performed before viral injection. The viral vector construction and injection were performed as previously reported.[51] Detailed information can be found in the Supplemental materials and methods.

Drugs and agents

We purchased the PKCα activator bryostatin-1 and the selective PKCα inhibitor Ro 32-0432 from Sigma-Aldrich (St. Louis, MO, USA). The GABA receptor blocker picrotoxin was from Tocris Bioscience (Ellisville, MO, USA). All drugs were dissolved in DMSO.

Statistical analysis

Data are presented as the mean ± SEM. The two-tailed Student's t test was applied for comparisons between two groups. Day-by-day between-group comparisons were performed by factorial ANOVA (split-plot design). One-way ANOVA was used for comparisons of more than two groups. Post hoc analyses of significant main effects were further examined with Tukey post hoc tests. All statistical analyses were performed with SAS 9.1 software (serial no. 989155; SAS Institute, Cary, NC, USA). Significance was accepted at $p < 0.05$, and graphs were generated with GraphPad Prism 5.0 software (La Jolla, CA, USA).

SUPPLEMENTAL INFORMATION

Supplemental Information can be found online at https://doi.org/10.1016/j.omtn.2021.02.015.

ACKNOWLEDGMENTS

This work was supported by the Key project of the Natural Science Foundation of Heilongjiang Province (ZD2018004), the Natural Science Foundation of China (81870849, 81671052, and 81471115 to J. A.), and the Heilongjiang Touyan Innovation Team Program.

AUTHOR CONTRIBUTIONS

J.A. and S.Z. designed research; S.Z., X.A., S.H., L.Z., Y.X., D.S., Y.Q., X.T., J.M. and J.Y. performed experiments; S.Z., X.A. and S.H., analyzed data; S.Z. and J.A. wrote the manuscript; and L.Z. provided valuable comments on the writing of the manuscript. All authors read and approved the final version of the manuscript.

DECLARATION OF INTERESTS

The authors declare no competing interests.

REFERENCES

1. Luine, V.N., and Frankfurt, M. (2012). Estrogens facilitate memory processing through membrane mediated mechanisms and alterations in spine density. Front. Neuroendocrinol. *33*, 388–402.
2. Hamson, D.K., Roes, M.M., and Galea, L.A. (2016). Sex Hormones and Cognition: Neuroendocrine Influences on Memory and Learning. Compr. Physiol. *6*, 1295–1337.
3. Yun, J., Yeo, I.J., Hwang, C.J., Choi, D.Y., Im, H.S., Kim, J.Y., Choi, W.R., Jung, M.H., Han, S.B., and Hong, J.T. (2018). Estrogen deficiency exacerbates Aβ-induced memory impairment through enhancement of neuroinflammation, amyloidogenesis and NF-κB activation in ovariectomized mice. Brain Behav. Immun. *73*, 282–293.
4. Lobo, R.A. (2017). Hormone-replacement therapy: current thinking. Nat. Rev. Endocrinol. *13*, 220–231.
5. Fioravante, D., Chu, Y., de Jong, A.P., Leitges, M., Kaeser, P.S., and Regehr, W.G. (2018). Retraction. eLife *7*, e35974.
6. Alkon, D.L., Sun, M.K., and Nelson, T.J. (2007). PKC signaling deficits: a mechanistic hypothesis for the origins of Alzheimer's disease. Trends Pharmacol. Sci. *28*, 51–60.
7. Colgan, L.A., Hu, M., Misler, J.A., Parra-Bueno, P., Moran, C.M., Leitges, M., and Yasuda, R. (2018). PKCα integrates spatiotemporally distinct Ca^{2+} and autocrine BDNF signaling to facilitate synaptic plasticity. Nat. Neurosci. *21*, 1027–1037.
8. Hongpaisan, J., and Alkon, D.L. (2007). A structural basis for enhancement of long-term associative memory in single dendritic spines regulated by PKC. Proc. Natl. Acad. Sci. USA *104*, 19571–19576.
9. Alfonso, S.I., Callender, J.A., Hooli, B., Antal, C.E., Mullin, K., Sherman, M.A., Lesné, S.E., Leitges, M., Newton, A.C., Tanzi, R.E., and Malinow, R. (2016). Gain-of-function mutations in protein kinase Cα (PKCα) may promote synaptic defects in Alzheimer's disease. Sci. Signal. *9*, ra47.
10. Salta, E., and De Strooper, B. (2012). Non-coding RNAs with essential roles in neurodegenerative disorders. Lancet Neurol. *11*, 189–200.
11. Sun, L.Y., Wang, N., Ban, T., Sun, Y.H., Han, Y., Sun, L.L., Yan, Y., Kang, X.H., Chen, S., Sun, L.H., et al. (2014). MicroRNA-23a mediates mitochondrial compromise in estrogen deficiency-induced concentric remodeling via targeting PGC-1α. J. Mol. Cell. Cardiol. *75*, 1–11.
12. Wang, N., Sun, L.Y., Zhang, S.C., Wei, R., Xie, F., Liu, J., Yan, Y., Duan, M.J., Sun, L.L., Sun, Y.H., et al. (2015). MicroRNA-23a participates in estrogen deficiency induced gap junction remodeling of rats by targeting GJA1. Int. J. Biol. Sci. *11*, 390–403.
13. Su, R., Dong, L., Zou, D., Zhao, H., Ren, Y., Li, F., Yi, P., Li, L., Zhu, Y., Ma, Y., et al. (2016). microRNA-23a, -27a and -24 synergistically regulate JAK1/Stat3 cascade and serve as novel therapeutic targets in human acute erythroid leukemia. Oncogene *35*, 6001–6014.
14. Wang, N., Tan, H.Y., Feng, Y.G., Zhang, C., Chen, F., and Feng, Y. (2018). microRNA-23a in Human Cancer: Its Roles, Mechanisms and Therapeutic Relevance. Cancers (Basel) *11*, 7.
15. Lin, S.T., Huang, Y., Zhang, L., Heng, M.Y., Ptácek, L.J., and Fu, Y.H. (2013). MicroRNA-23a promotes myelination in the central nervous system. Proc. Natl. Acad. Sci. USA *110*, 17468–17473.
16. Zhu, X., Zhang, A., Dong, J., Yao, Y., Zhu, M., Xu, K., and Al Hamda, M.H. (2019). MicroRNA-23a contributes to hippocampal neuronal injuries and spatial memory impairment in an experimental model of temporal lobe epilepsy. Brain Res. Bull. *152*, 175–183.
17. Rataj, F., Möller, F.J., Jähne, M., Hönscheid, P., Zierau, O., Vollmer, G., and Kretzschmar, G. (2015). Progesterone, as well as 17β-estradiol, is important for regulating AHR battery homoeostasis in the rat uterus. Arch. Toxicol. *89*, 393–404.
18. Rataj, F., Möller, F.J., Jähne, M., Zierau, O., Diel, P., Vollmer, G., and Kretzschmar, G. (2012). Regulation of uterine AHR battery gene expression by 17β-Estradiol is predominantly mediated by estrogen receptor α. Arch. Toxicol. *86*, 1603–1612.
19. Dutta, S., and Sengupta, P. (2016). Men and mice: Relating their ages. Life Sci. *152*, 244–248.
20. Georgakis, M.K., Kalogirou, E.I., Diamantaras, A.A., Daskalopoulou, S.S., Munro, C.A., Lyketsos, C.G., Skalkidou, A., and Petridou, E.T. (2016). Age at menopause and duration of reproductive period in association with dementia and cognitive function: A systematic review and meta-analysis. Psychoneuroendocrinology *73*, 224–243.
21. Bosch, M., Castro, J., Saneyoshi, T., Matsuno, H., Sur, M., and Hayashi, Y. (2014). Structural and molecular remodeling of dendritic spine substructures during long-term potentiation. Neuron *82*, 444–459.
22. Sun, M.K., and Alkon, D.L. (2014). The "memory kinases": roles of PKC isoforms in signal processing and memory formation. Prog. Mol. Biol. Transl. Sci. *122*, 31–59.
23. Sun, M.K., Hongpaisan, J., Nelson, T.J., and Alkon, D.L. (2008). Poststroke neuronal rescue and synaptogenesis mediated in vivo by protein kinase C in adult brains. Proc. Natl. Acad. Sci. USA *105*, 13620–13625.
24. Ito, A., Saito, N., Hirata, M., Kose, A., Tsujino, T., Yoshihara, C., Ogita, K., Kishimoto, A., Nishizuka, Y., and Tanaka, C. (1990). Immunocytochemical localization of the alpha subspecies of protein kinase C in rat brain. Proc. Natl. Acad. Sci. USA *87*, 3195–3199.

25. Harris, J.A., Devidze, N., Halabisky, B., Lo, I., Thwin, M.T., Yu, G.Q., Bredesen, D.E., Masliah, E., and Mucke, L. (2010). Many neuronal and behavioral impairments in transgenic mouse models of Alzheimer's disease are independent of caspase cleavage of the amyloid precursor protein. J. Neurosci. *30*, 372–381.

26. Ansonoff, M.A., and Etgen, A.M. (1998). Estradiol elevates protein kinase C catalytic activity in the preoptic area of female rats. Endocrinology *139*, 3050–3056.

27. Drouva, S.V., Gorenne, I., Laplante, E., Rérat, E., Enjalbert, A., and Kordon, C. (1990). Estradiol modulates protein kinase C activity in the rat pituitary in vivo and in vitro. Endocrinology *126*, 536–544.

28. Satoh, M., Nasu, T., Takahashi, Y., Osaki, T., Hitomi, S., Morino, Y., and Nakamura, M. (2017). Expression of mir-23a induces telomere shortening and is associated with poor clinical outcomes in patients with coronary artery disease. Clin. Sci. (Lond.) *131*, 2007–2017.

29. Luo, Z., Feng, X., Wang, H., Xu, W., Zhao, Y., Ma, W., Jiang, S., Liu, D., Huang, J., and Songyang, Z. (2015). Mir-23a induces telomere dysfunction and cellular senescence by inhibiting TRF2 expression. Aging Cell *14*, 391–399.

30. Dal-Pan, A., Dudonné, S., Bourassa, P., Bourdoulous, M., Tremblay, C., Desjardins, Y., and Calon, F.; Neurophenols Consortium (2017). Cognitive-Enhancing Effects of a Polyphenols-Rich Extract from Fruits without Changes in Neuropathology in an Animal Model of Alzheimer's Disease. J. Alzheimers Dis. *55*, 115–135.

31. Fehlmann, T., Kahraman, M., Ludwig, N., Backes, C., Galata, V., Keller, V., Geffers, L., Mercaldo, N., Hornung, D., Weis, T., et al. (2020). Evaluating the Use of Circulating MicroRNA Profiles for Lung Cancer Detection in Symptomatic Patients. JAMA Oncol. *6*, 714–723.

32. Karakas, M., Schulte, C., Appelbaum, S., Ojeda, F., Lackner, K.J., Münzel, T., Schnabel, R.B., Blankenberg, S., and Zeller, T. (2017). Circulating microRNAs strongly predict cardiovascular death in patients with coronary artery disease-results from the large AtheroGene study. Eur. Heart J. *38*, 516–523.

33. Westphal, M., and Lamszus, K. (2015). Circulating biomarkers for gliomas. Nat. Rev. Neurol. *11*, 556–566.

34. Melman, Y.F., Shah, R., Danielson, K., Xiao, J., Simonson, B., Barth, A., Chakir, K., Lewis, G.D., Lavender, Z., Truong, Q.A., et al. (2015). Circulating MicroRNA-30d Is Associated With Response to Cardiac Resynchronization Therapy in Heart Failure and Regulates Cardiomyocyte Apoptosis: A Translational Pilot Study. Circulation *131*, 2202–2216.

35. Szabo, G., and Bala, S. (2013). MicroRNAs in liver disease. Nat. Rev. Gastroenterol. Hepatol. *10*, 542–552.

36. Siedlecki-Wullich, D., Català-Solsona, J., Fábregas, C., Hernández, I., Clarimon, J., Lleó, A., Boada, M., Saura, C.A., Rodríguez-Álvarez, J., and Miñano-Molina, A.J. (2019). Altered microRNAs related to synaptic function as potential plasma biomarkers for Alzheimer's disease. Alzheimers Res. Ther. *11*, 46.

37. Hara, N., Kikuchi, M., Miyashita, A., Hatsuta, H., Saito, Y., Kasuga, K., Murayama, S., Ikeuchi, T., and Kuwano, R. (2017). Serum microRNA miR-501-3p as a potential biomarker related to the progression of Alzheimer's disease. Acta Neuropathol. Commun. *5*, 10.

38. Li, X., Chen, W., Pan, K., Li, H., Pang, P., Guo, Y., Shu, S., Cai, Y., Pei, L., Liu, D., et al. (2018). Serotonin receptor 2c-expressing cells in the ventral CA1 control attention via innervation of the Edinger-Westphal nucleus. Nat. Neurosci. *21*, 1239–1250.

39. Chen, G., Zou, X., Watanabe, H., van Deursen, J.M., and Shen, J. (2010). CREB binding protein is required for both short-term and long-term memory formation. J. Neurosci. *30*, 13066–13077.

40. Saraf, A., Luo, J., Morris, D.R., and Storm, D.R. (2014). Phosphorylation of eukaryotic translation initiation factor 4E and eukaryotic translation initiation factor 4E-binding protein (4EBP) and their upstream signaling components undergo diurnal oscillation in the mouse hippocampus: implications for memory persistence. J. Biol. Chem. *289*, 20129–20138.

41. Huang, C.H., Yu, Y.J., Chang, C.H., and Gean, P.W. (2016). Involvement of metabotropic glutamate receptor 5 in the inhibition of methamphetamine-associated contextual memory after prolonged extinction training. J. Neurochem. *137*, 216–225.

42. Dai, J., Aoto, J., and Südhof, T.C. (2019). Alternative Splicing of Presynaptic Neurexins Differentially Controls Postsynaptic NMDA and AMPA Receptor Responses. Neuron *102*, 993–1008.e5.

43. Guo, Y., Zhao, M., Bo, T., Ma, S., Yuan, Z., Chen, W., He, Z., Hou, X., Liu, J., Zhang, Z., et al. (2019). Blocking FSH inhibits hepatic cholesterol biosynthesis and reduces serum cholesterol. Cell Res. *29*, 151–166.

44. Zhu, H., Wang, N., Yao, L., Chen, Q., Zhang, R., Qian, J., Hou, Y., Guo, W., Fan, S., Liu, S., et al. (2018). Moderate UV Exposure Enhances Learning and Memory by Promoting a Novel Glutamate Biosynthetic Pathway in the Brain. Cell *173*, 1716–1727.e17.

45. Leger, M., Quiedeville, A., Bouet, V., Haelewyn, B., Boulouard, M., Schumann-Bard, P., and Freret, T. (2013). Object recognition test in mice. Nat. Protoc. *8*, 2531–2537.

46. Pitts, M.W. (2018). Barnes Maze Procedure for Spatial Learning and Memory in Mice. Bio Protoc. *8*, e2744.

47. Yan, M.L., Zhang, S., Zhao, H.M., Xia, S.N., Jin, Z., Xu, Y., Yang, L., Qu, Y., Huang, S.Y., Duan, M.J., et al. (2020). MicroRNA-153 impairs presynaptic plasticity by blocking vesicle release following chronic brain hypoperfusion. Cell Commun. Signal. *18*, 57.

48. Chen, X., Jiang, X.M., Zhao, L.J., Sun, L.L., Yan, M.L., Tian, Y., Zhang, S., Duan, M.J., Zhao, H.M., Li, W.R., et al. (2017). MicroRNA-195 prevents dendritic degeneration and neuron death in rats following chronic brain hypoperfusion. Cell Death Dis. *8*, e2850.

49. Zhang, S., Yan, M.L., Yang, L., An, X.B., Zhao, H.M., Xia, S.N., Jin, Z., Huang, S.Y., Qu, Y., and Ai, J. (2020). MicroRNA-153 impairs hippocampal synaptic vesicle trafficking via downregulation of synapsin I in rats following chronic cerebral hypoperfusion. Exp. Neurol. *332*, 113389.

50. Knafo, S., Sánchez-Puelles, C., Palomer, E., Delgado, I., Draffin, J.E., Mingo, J., Wahle, T., Kaleka, K., Mou, L., Pereda-Perez, I., et al. (2016). PTEN recruitment controls synaptic and cognitive function in Alzheimer's models. Nat. Neurosci. *19*, 443–453.

51. Ai, J., Sun, L.H., Che, H., Zhang, R., Zhang, T.Z., Wu, W.C., Su, X.L., Chen, X., Yang, G., Li, K., et al. (2013). MicroRNA-195 protects against dementia induced by chronic brain hypoperfusion via its anti-amyloidogenic effect in rats. J. Neurosci. *33*, 3989–4001.